Journal of Power Sources 244 (2013) 521–526

Contents lists available at SciVerse ScienceDirect

Journal of Power Sources

journal homepage: www.elsevier.com/locate/jpowsour

Short communication

Effect of polyimide binder on electrochemical characteristics of surface-modified silicon anode for lithium ion batteries

Jung Sub Kim [a,b], Wonchang Choi [a], Kyu Young Cho [a,c], Dongjin Byun [b], JongChoo Lim [c], Joong Kee Lee [a,*]

[a] Center for Energy Convergence, Korea Institute of Science and Technology, Hwarangno 14-gil 5, Seongbuk-gu, Seoul 136-791, Republic of Korea
[b] Department of Material Science & Engineering, Korea University, Seoul 136-713, Republic of Korea
[c] Department of Chemical and Biochemical Engineering, Dongguk University-Seoul, 3-26 Pil-Dong, Chung-Gu, Seoul 100-715, Republic of Korea

HIGHLIGHTS

- Si nanostructures are prepared by Ag-assisted chemical etching.
- The choice of PI binder for Si nanostructure is very important.
- The employment of PI binder improves electrochemical performance.
- The mechanical properties of PI mitigate the volume change of Si electrode.
- The proper selection of binders such as polyimide is one of the key factors.

ARTICLE INFO

Article history:
Received 31 October 2012
Received in revised form
13 February 2013
Accepted 15 February 2013
Available online 26 February 2013

Keywords:
Silicon
Anode
Binder
Lithium ion battery

ABSTRACT

Si nanostructures with high surface area are prepared by Ag-assisted chemical etching, and then employed as an anode material for lithium ion batteries. The use of the surface-modified Si, which has four times higher surface area than its pristine counterpart, leads to the enhancement of electrochemical performance characteristics such as discharge capacity and coulombic efficiency. In order to optimize the electrode constituents, two different binders, poly-vinylidine difluoride (PVdF) and polyimide (PI), are evaluated on the basis of electrochemical and physical tests. In-situ dilatometer and nano-indentation studies during repeated charging and discharging cycles for the different binders reveal more stability and recuperative capability against physical stress with the PI binder than with the PVdF. The optimized active structure combined with the film-like binder plays an important role in enhancing the electrochemical performance.

1. Introduction

Graphite is used as an anode material for lithium ion batteries, because of its superior cycle stability compared with other anode materials. However, the theoretical capacity of graphite is limited to 372 mAh g^{-1}. To develop rechargeable lithium batteries with high energy density, intensive studies have focused on silicon anode materials due to their extremely high lithium storage of about 4200 mAh g^{-1}, and low discharge potential [1,2]. However, the commercial use of Si-based power is still hindered, because of two major problems. One is the low electrical conductivity of Si, and the other is the volume expansion during the charge and discharge (lithiation and delithiation) of Li^+. The repeated mechanical fatigue of Si-based anodes upon prolonged cycling leads to a loss of capacity and poor cycle life.

Important approaches to resolve these problems include the control of Si surface morphologies. Several approaches of surface modification can be considered to enhance the capacity retention, including carbon–silicon core-shell nanowires, Si nanotubes, Si nanowires, and Si hollow nanospheres [3–6]. Recently, metal-assisted chemical etching has become attractive for modifying the surface of silicon based on galvanic displacement [7]. The galvanic displacement process, the reduction of oxidizing metal ions to metallic species such as particles and film, and the dissolution of silicon atoms act as a reducing agent for metal ions in an aqueous HF solution [8]. These active materials have high surface area. The active materials of nanostructures with high surface area play important roles in the binder. From a practical point of view,

* Corresponding author.
E-mail addresses: leejk@kist.re.kr, joongkee57@naver.com (J.K. Lee).

0378-7753/$ – see front matter © 2013 Elsevier B.V. All rights reserved.
http://dx.doi.org/10.1016/j.jpowsour.2013.02.049

surface-modified Si powder materials ultimately need to be incorporated with conducting material and binder to make a commercially viable composite negative electrode. Thus, the effect of the binder that holds the materials together on the electrode performance needs to be considered. For commercial lithium ion batteries, polyvinylidene fluoride (PVdF) has been used as a binder for both the anode and cathode due to its good electrochemical stability. However, the mechanical properties of PVdF binder are not sufficient to accommodate the significant volume change in the Si electrode. In one trial, Chen et al. [9–11] and Liu et al. [12] showed that the selection of binder is very important for the electrochemical performance of anode electrodes. So far, candidates for various new binders for Si anodes have included styrene butadiene rubber–sodium carboxymethyl cellulose (SBR–SCMC), sodium carboxymethyl cellulose (SCMC), polyamide imide (PAI), and polyacrylic acid (PAA), among others [12–18].

The purpose of this work is to investigate the effect of polyimide (PI) binder compared with PVdF in an etched Si anode with high surface area. Surface-modified Si anodes with high surface area will not only offer favorable free vacancies, but also act against volume change. Furthermore, PI binder will be compatible with the surface-modified Si anodes.

2. Experimental

2.1. Preparation of modified Si

Surface-modified Si is prepared by Ag-assisted chemical etching. In order to etch the Si powder, commercially available Si powder (Kojundo co., 5 μm of average size, 99.9%) is dispersed in an etching solution that consists of 49 wt.% hydrofluoric acid (2.5 mol L^{-1}), 60 wt.% nitric acid (0.036 mol L^{-1}) and de-ionized water. The etching solution is mildly stirred for 1 h in order to prevent the detachment of Ag. After the etching process, the silver nanoparticles are removed from the silicon powder using a 50 wt.% HNO_3 aqueous solution, and the etched silicon powders are filtered out from the etching solution and dried in a vacuum oven at 100 °C for 10 h.

2.2. Cell fabrication

A working electrode is prepared by coating slurries containing pristine and etched Si as active material (50, 46, 42.5 wt.%), Denka black (DB) as a conducting agent (40, 36, 32.5 wt.%), and PVdF (10 wt.%) or PI (10, 18, 25 wt.%) as binders dissolved in *N*-methyl-2-pyrrolidinone (NMP) on a copper foil current collector. The high amount of carbon not only helps the electric conductivity, but also prevents volume change. After solvent evaporation, the electrode is rolled and dried in a vacuum oven at 100 °C for 6 h. The weight of the final active material, which has a thickness of 50 μm, is in the range of 4.4–4.8 mg cm^{-3}. CR2032 coin-type half cells are assembled and sealed in a dry room whose moisture content is maintained at less than 0.5%. The test cells comprise a working electrode, lithium foil as the counter electrode, and polypropylene (PP) membrane as a separator. The liquid electrolyte is 1 M $LiPF_6$ dissolved in a mixture of ethylene carbonate (EC), ethylmethyl carbonate (EMC), and dimethyl carbonate (DMC) (1:1:1 in vol%). To find the reactivity of PVdF and PI during the insertion and extraction of Li^+, a DB electrode (1.9 mg cm^{-3}) is also fabricated by coating slurries active material (90 wt.%) and PVdF and PI binder (10%).

2.3. Characterization

SEM studies of the pristine Si and etched Si powder are carried out using field emission scanning electron microscope (FESEM, NOVA NANO SEM200, FEI co.). The secondary electron detector is used for the studies, most of which are performed using an accelerating voltage of 10 kV and a working distance of 5–5.5 mm. The surface areas are measured by the Brunauer Emmett Teller (BET) method, using an N_2 sorption isotherm plot measured on a Micromeritics apparatus (ASAP 2010) in order to compare the

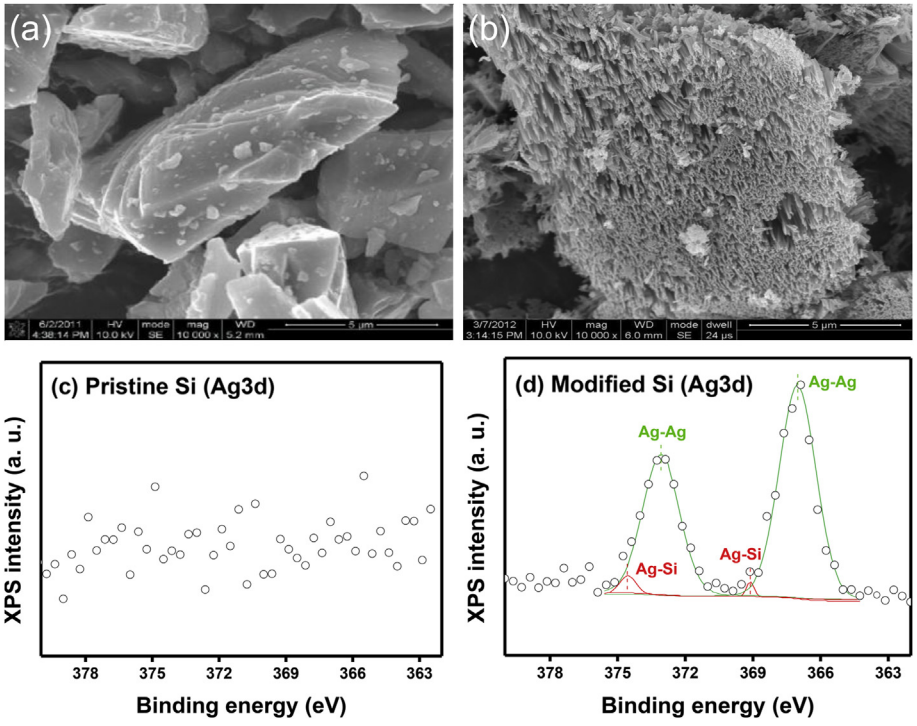

Fig. 1. SEM images and XPS spectra of preparation process with different treatments: (a, c) pristine Si power, (b, d) after Ag-assisted chemical etching.

Table 1
Comparison of atomic percent of various elements between pristine and etched Si.

Active material	Atomic percent of various elements					
	Cls (%)	Ols (%)	Fls (%)	Ag3d (%)	Si2p (%)	Ag/Si ratio
Pristine Si	15.07	44.08	0	0	40.85	0
Etched Si	17.49	39.41	0.14	0.21	42.75	0.0049

changes in surface area before and after etching. For chemical bond and compositional analysis, X-ray Photoelectron Spectroscopy (XPS, PHI 5000 VersaProbe) with a background pressure of 6.7×10^{-8} Pa is carried out in Ar atmosphere. Galvanostatic charge–discharge cycling tests for the testing of electrical and chemical properties are carried out on a Maccor automated battery tester (MACCOR series-4000) in the potential range of 0–2 V (vs. Li/Li^+) at a current density of 200 mA g^{-1}. All measurements are performed at room temperature. Electrochemical impedance spectroscopy (EIS) experiments with the fully discharged (up to 2 V) cells are performed using an impedance/gain-phase analyzer (Solartron SI 1260) equipped with an electrochemical interface (Solartron SI 1286). The AC amplitude is 5 mV, with a frequency range of 1–10^6 Hz.

Mechanical properties such as the modulus and hardness of the PVdF and PI binder are investigated by nano-indentation measurement (Agilent Technologies, Inc.). Polymeric film with a thickness of 5 μm is coated onto an Si wafer by spin coating with fixed coating conditions. Thicker films are needed to avoid the influence of the underlying substrate on the measurements. During the measurement, a sharp diamond indenter is forced (4 mN min^{-1} of loading and unloading rate) into the tested material while continuously recording both the force (2 mN of max force) and the indentation depth.

The volume change is estimated using an in-situ dilatometer with a gap sensor (Solartron, DT-2S) on a non-vibration table. The displacement (with an error range of about 0.2 μm) is recorded as a function of time with simultaneous electrochemical reaction.

3. Results and discussion

As shown in Fig. 1, top-view images are observed to investigate the surface morphologies of Si powder prepared by Ag-assisted chemical etching. Fig. 1(a) shows SEM images of pristine Si powder with a size of approximately 5 μm and smooth surfaces. After filtration, the Ag particles aggregate with each other on the Si surface. Then, the Ag component is removed using a 50 wt.% HNO_3 aqueous solution, as shown in Fig. 1(b). After Ag removal, the Si surface has different morphology, with nanorod and porous shapes. The BET surface areas of pristine and modified Si are 1.72 and 7.0 m^2 g^{-1}, respectively. Fig. 1(c and d) shows the XPS spectra of pristine (c) and modified Si surfaces (d) in the Ag 3d region. The peaks are fitted by a Gaussian–Lorenz function. The fitting data is superior (chi-square of fitting results). As shown in Fig. 1(c), Ag is not observed in pristine Si (atomic concentration: 0%). On the other hand, peaks of modified Si can be observed around 373 and 367 eV, which originates from Ag $3d_{3/2}$ and $3d_{5/2}$, respectively [19]. In the literature, the XPS spectrum includes Ag–Ag and Ag–Si bonds at low concentration of $AgNO_3$. However, an Ag–O bond is observed with increasing $AgNO_3$ concentration due to the high thickness of Ag [20]. In modified Si, the Ag–O peak is not observed, as shown in Fig. 1(d). The result shows that the amount of Ag is very small in the Si surface, as shown in Table 1 (atomic concentration: 0.21%, relative Ag/Si ratio: 0.0049). Moreover, F impurity (0.14%) is observed in the etched Si due to the HF solution.

Fig. 2(a) presents the charge–discharge profiles of pristine and modified Si electrodes in the potential range of 0–2 V at a current density of 200 mA g^{-1}. All cell tests are carried out at nearly 100% depth of discharge (DOD) during cycling and with no limit to the insertion capacity. The pristine silicon anode shows charge and discharge capacities of 1987 and 1536 mAh g^{-1}, respectively, with a coulombic efficiency of 77.3% in the first cycle. In the second cycle, the charge–discharge capacities are decreased to 1545 and 1370 mAh g^{-1}, respectively, with a coulombic efficiency of 88.6%, as shown in Table 2. In comparison, the surface-modified Si electrode with a different morphology shows a relatively high reversible capacity of 1782 mAh g^{-1} during Li^+ extraction. Furthermore, the coulombic efficiencies of the surface-modified Si anode (81.5, 92%) are greater than those of the pristine Si anode (77.3, 88.6%) during the first and second cycles, as shown in Table 2 and Fig. 2(a). At the first cycle, the voltage profiles are quite different as a result of changes in crystal structure. As shown in Fig. 2(a), Christensen et al. reported that the charging profiles have two different voltage regions, from 100 to 70 mV and 70 to 5 mV, respectively, due to phase transition from crystalline to amorphous and amorphous changes to $Li_{15}Si_4$ [21]. These phase transitions induced a large volume expansion of the active Si material, resulting in the decline of the electrical conduction network. The morphology of the Si powder with high surface area plays an important role in minimizing the deterioration of the electrical contact between the Si particles and conducting agent, because of free spaces that act against volume change. Fig. 2(b) compares the degree of cycle degradation of the pristine and etched Si powder used as anode electrodes. In the case

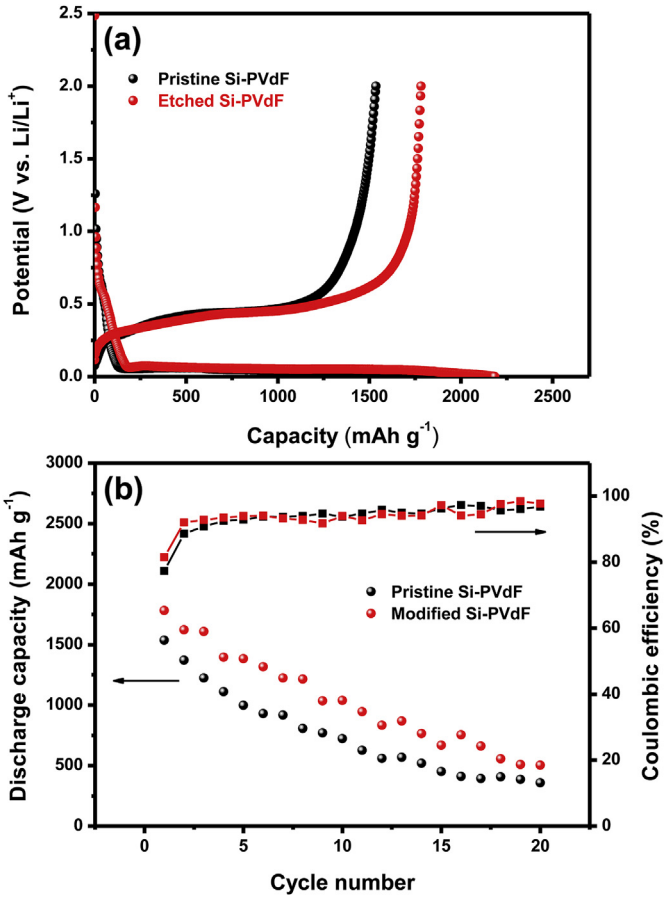

Fig. 2. Voltage profiles (a) and discharge capacities (b) of pristine and modified Si in a potential range of 0–2 V at a current density of 200 mA g^{-1}.

Table 2
Charge–discharge capacities and coulombic efficiencies of pristine Si–PVdF, etched Si–PVdF and etched Si–PI at first and second cycles.

Active material-binder	1st cycle capacity (mAh g^{-1})		2nd cycle capacity (mAh g^{-1})		Coulombic efficiency (%)	
	Charge	Discharge	Charge	Discharge	1st cycle	2nd cycle
Pristine Si–PVdF	1987	1536	1545	1370	77.3	88.6
Etched Si–PVdF	2184	1782	1762	1622	81.5	92.0
Etched Si–PI	2565	2077	2274	2175	81.0	95.6

of pristine Si, the discharge capacity was rapidly diminished after 1 cycle. The fading process began after phase change and resulted in a decrease of the discharge capacity of ca. 76% after 20 cycles. This result can be attributed to the cracking of the Si anode because of the volume extension during lithium insertion. Although the voltage profile result was slightly better than that of pristine Si, the cycle retention of modified Si is unsatisfactory. From these results, the etched Si powder with high surface area as an active material is selected to examine the binder effects with PI and PVdF.

The literature exhibits reaction of the C=O group of the imide ring in PI and polyamide imide (PAI) binder with Li^+ and e^- [15,22]. Because PI and PAI binders react with Li^+ and e^- during Li^+ insertion, the capacities of electrodes using PI and PAI binder were improved. To verify the results, a Denka black (DB) electrode is preliminarily applied with different binders, as shown in Fig. 3(a). The discharge capacity with PI binder is improved by about 80 mAh g^{-1} due to the reaction of the carboxyl group. It is suggested based on our results that PI binders, which are electrochemically active rather than inert, are effective for improving battery performance. Fig. 3(b) shows the curve of potential vs. specific capacity during the first cycle of etched silicon anodes using PVdF and PI binders in the potential range of 0–2 V (vs. Li/Li^+) at current densities of 200 mA g^{-1}. The etched silicon anode with PVdF shows a charge and discharge capacity of 2184 and 1762 mAh g^{-1}, respectively, with a coulombic efficiency of 80.7% in the first cycle. However, the reversible capacity of the second cycle is decreased to 1622 mAh g^{-1}, as shown in Table 2. The charge–discharge capacities of the first and second cycles of the etched Si–PI electrodes are 2565, 2077, and 2274, 2175 mAh g^{-1}, indicating coulombic efficiencies of 81 and 95.6%, respectively. In comparison with the etched Si–PVdF electrode, the etched Si–PI electrodes show a relatively high capacity (315 mAh g^{-1}) and greater coulombic efficiency, as shown Table 2. More interestingly, the discharge capacities in the case of Si–PI electrodes increase about 315 mAh g^{-1}, in contrast with DB-PI electrodes (80 mAh g^{-1}). In the case of the Si electrode with volume change, the discharge capacity of the Si nanostructure combined with PI binder is increased due to reduced capacity loss caused by physical stress. Fig. 3(c) presents voltage profiles of etched Si electrodes with different amounts of PI binder (10, 18 and 25%). The charge–discharge capacities increased with the amounts of PI binder, because a high content of PI binder has quite a few active carboxyl groups. However, the cycle retention (not shown) with a high amount of the binder is not effective, owing to the resistance of the electrode. To identify the resistance, we employ impedance spectroscopy techniques, and address data obtained from Nyquist plots, where the imaginary part of the impedance is plotted as a function of the real part over a wide range of frequencies, as shown in Fig. 3(d). We measure the impedance spectra of Si electrodes with different amounts of PI after the initial cycle, in a frequency range between 1 and 10^6 Hz the equivalent circuits utilized in the impedance analyses are given in the inset of Fig. 3(d), where R_E is the resistance of the bulk electrolyte, Q_{SEI} is the space charge capacitance of the SEI layer, and R_{SEI} is the resistance for Li^+ conduction in the SEI layer. R_{CT}, Q_{DL}, and Z_W represent the

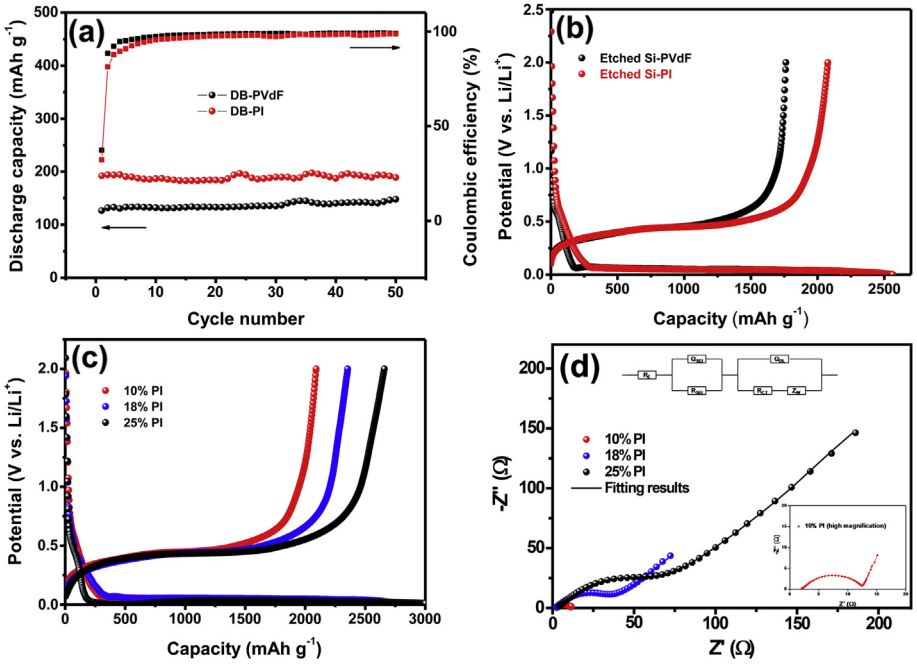

Fig. 3. (a) Discharge capacities of DB electrode (1.9 mg cm^{-3}) as a function of cycle number with different binders (PVdF and PI) in a potential range of 0–2 V, (b) Comparison of the voltage profiles with different binders (Si–PVdF and Si–PI) in a potential range of 0–2 V at a current density of 200 mA g^{-1}, (c) initial charge–discharge profiles with contents of PI (10, 18 and 25%), (d) after 1 cycle, EIS measurement with contents of PI (10, 18 and 25%, inset figure: high magnification of 10% PI).

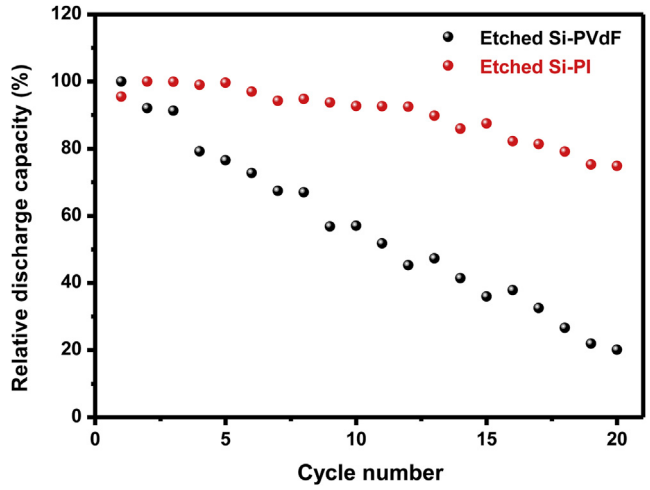

Fig. 4. Relative discharge capacities of different binders (PVdF and PI) in a potential range of 0–2 V at a current density of 200 mA g^{-1}.

charge transfer resistance, double-layer capacitance at the electrode surface, and the Warburg impedance, respectively. It is generally known that the semicircles in the high frequency region reflect the interfacial characteristics of electrodes, whereas the straight line in the low frequency region is related to the Warburg diffusion of lithium ions in the electrochemical cells including Si electrodes [23]. As shown in Fig. 3(d), it is clear that the diameter of the semicircle for the case of the electrode with a low amount of PI (8 Ω cm^2) is much smaller than that for the case with a high amount (66 Ω cm^2). Although the reversible capacity increased with the amount of PI binder, an excessively high amount of PI cannot be used due to an increase of the charge transfer resistance. From these results, the PI binder with 10% content is selected for binder effect in the surface-modified Si with high surface area.

The relative discharge capacities during 20 cycles of the etched silicon anodes using PI and PVdF binders (10%) are shown in Fig. 4. In terms of capacity retention, the etched silicon anodes using PI binder are better than those using PVdF binder. The capacities of PVdF binder decline more steeply than with PI binder, and after 20 cycles, the PI binder (75.9%) retains a considerably higher capacity than the PVdF binder (20.1%). Although PVdF is an excellent binder to carbon materials (volume change of about 10%), it has poor mechanical properties with collector metals. As a result, during repeated lithium

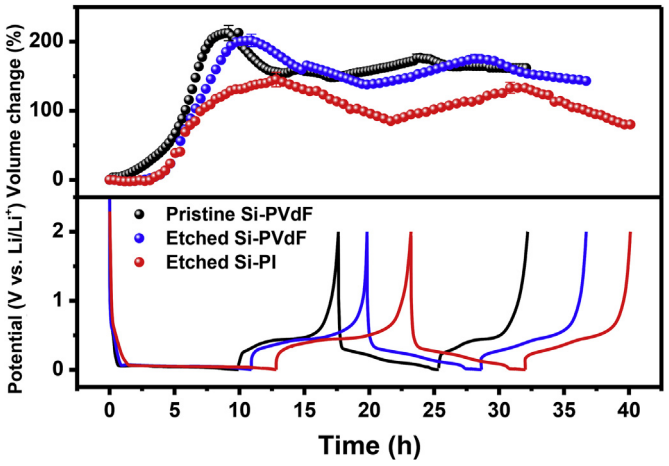

Fig. 5. Voltage profiles and volume change (%) vs. total time of pristine Si–PVdF, etched Si–PVdF and etched Si–PI electrode measured by in-situ electrochemical dilatometer.

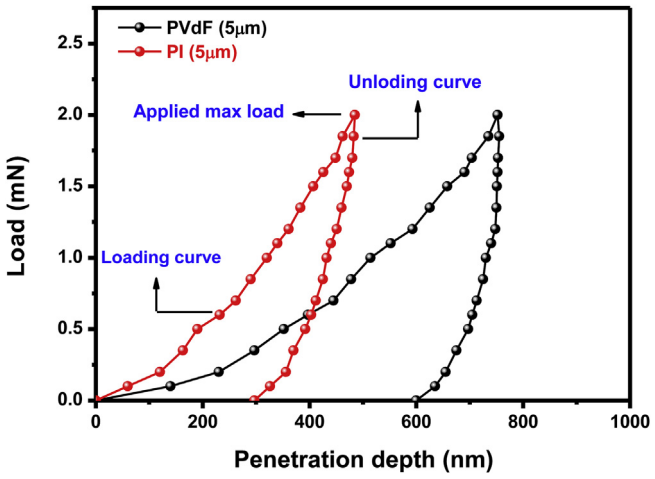

Fig. 6. Load-penetration depth curves for 2 mN in 5 μm PVdF and PI on Si wafer.

ion insertion and extraction, the carbon powder used peels off from the collector metals such as copper plate or copper foil, thereby gradually decreasing the battery capacity. For Si electrodes, volumetric changes are substantially greater than those of carbon materials. Therefore, the PVdF binder is not efficient in Si electrodes because of its mechanical properties against volumetric changes.

Guerfi et al. observed the volume change of SiO_x-graphite electrodes (PI binder) using in-situ SEM [24]. In our case, in-situ dilatometer measurements are carried out for volume changes of Si with different binders, as shown in Fig. 5. When the potential moves from 2.0 to 0.26 V, all electrodes show slight dilation. However, when the cell is charged (Li^+ insertion) from 0.26 to 0 V, the thickness of the Si-based electrode is increased significantly. Upon discharging (Li^+ extraction) the cell, considerable decrease of the electrode thickness from 0 to 0.45 V takes place. The rate of shrinkage is slow again in a potential range 0.45–2 V. The conversion point from dilation is well matched with charge–discharge curves. The volume changes of pristine Si–PVdF and etched Si–PVdF electrodes are evaluated to be about 212 and 201% at the first cycle, respectively. On the other hand, the volume change of the etched Si with PI binder is decreased down to 145%. All electrodes reveal error ranges between 6 and 10.5% in experimental repetition. According to the graphs, a smaller volume change and a slower rate of expansion in the etched Si–PI electrodes are also the main causes for the improvement of cyclic ability of the electrodes. In other words, the improvement of electrochemical performance originated from the application of the PI binder due to the binder's mechanical properties. The in-situ electrochemical dilatometric method is useful for identifying the relation between the expansion behavior and electrochemical performance.

To measure the mechanical properties of the binder, indentation loads of 2 mN are applied, and the hardness and the modulus are determined by applying the Oliver–Pharr method to load-penetration [25]. In order to extract values, high thickness of polymer film is used, because of the removal of the substrate effect. The test is also performed with a sharp indenter (Berkovich). Fig. 6 shows the load-penetration depth curves of PVdF and PI. The elastic recoveries are 39% for PI and 21% for PVdF. The elastic modulus and Vickers hardness of the PI binder are evaluated as about 7.5 GPa and 43.8 HV, respectively. The elastic modulus and Vickers hardness of PI were higher than those of PVdF (6.4 GPa, 15.5 HV). These results suggest that PI binder plays an important role in mitigating the physical volume change during the insertion and extraction of Li^+. Due to their mechanical properties, the volume change of the electrode with PI is greatly reduced, and the electric conduction

network is well maintained, which eventually yields much improved cycle performance. The mechanical properties of PI might affect the electrochemical performance of the Si electrode by reducing the volume change during cycling.

4. Conclusions

In order to mitigate the volume change during the charge–discharge process, Si nanostructures with free vacancies and high surface area were prepared by Ag-assisted chemical etching processes, and then employed as an anode material for lithium ion batteries. The electrochemical performances of the Si nanostructures using PVdF binder were unsatisfactory due to its unstable characteristics in an electrochemical environment. The PVdF binder is not efficient in the surface-modified Si electrode because of the weak mechanical properties of the Van-der-Waals bonding against volumetric changes. Surprisingly, the introduction of PI binder improved the electrochemical performances of the Si electrodes. Further investigation with dilatometer and nanoindentation studies revealed that the physical stress of the etched Si–PI electrode caused by induced phase transition in the alloy reaction of Li^+ is suppressed, which improves the electrochemical performance of the Si electrodes with high surface area. Indeed, the proper selection of binders such as polyimide is one of the key factors for enhancing the electrochemical performances of Li-alloying materials, especially for those with high surface area.

Acknowledgments

This work was supported by the National Research Foundation of Korea Grant funded by the Korean Government (MEST) (NRF-2010-C1AAA001-2010-0028958)

References

[1] C.J. Wen, R.A. Huggins, J. Solid State Chem. 37 (1981) 271–278.
[2] B.A. Boukamp, G.C. Lesh, R.A. Huggins, R. Smith, J. Electrochem. Soc. 128 (1981) 725–729.
[3] L.-F. Cui, Y. Yang, C.-M. Hsu, Y. Cui, Nano Lett. 9 (2009) 3370–3374.
[4] H. Wu, G. Chan, J.W. Choi, I. Ryu, Y. Yao, M.T. McDowell1, S.W. Lee, A. Jackson, Y. Yang, L. Hu, Y. Cui, Nat. Nanotechnol. 7 (2012) 310–315.
[5] C.K. Chan, H. Peng, G. Liu, K. Mcilwrath, X.F. Zhang, R.A. Huggins, Y. Cui, Nat. Nanotechnol. 3 (2008) 31–35.
[6] Y. Yao, M.T. McDowell, I. Ryu, H. Wu, N. Liu, L. Hu, W.D. Nix, Y. Cui, Nano Lett. 11 (2011) 2949–2954.
[7] X. Li, P.W. Bohn, Appl. Phys. Lett. 77 (2000) 2572–2574.
[8] T. Unagami, J. Electrochem. Soc. 127 (1980) 476–483.
[9] Z. Chen, V. Chevrier, L. Christensen, J.R. Dahn, Electrochem. Solid State Lett. 7 (2004) A310–A314.
[10] Z. Chen, L. Christensen, J.R. Dahn, J. Electrochem. Soc. 150 (2003) A1073–A1078.
[11] Z. Chen, L. Christensen, J.R. Dahn, Electrochem. Commun. 5 (2003) 919–923.
[12] W.R. Liu, M.H. Yang, H.C. Wu, S.M. Chiao, N.-L. Wu, Electrochem. Solid State Lett. 8 (2005) A100–A103.
[13] J. Li, R.B. Lewis, J.R. Dahn, Electrochem. Solid State Lett. 10 (2007) A17–A20.
[14] J.-S. Bridel, T. Azaïs, M. Morcrette, J.-M. Tarascon, D. Larcher, Chem. Mater. 22 (2010) 1229–1241.
[15] N.-S. Choi, K.H. Yew, W.-U. Choi, S.-S. Kim, J. Power Sourc. 177 (2008) 590–594.
[16] A. Magasinski, B. Zdyrko, I. Kovalenko, B. Hertzberg, R. Burtovyy, C.F. Huebner, T.F. Fuller, I. Luzinov, G. Yushin, ACS Appl. Mater. Interfaces 2 (2010) 3004–3010.
[17] N. Ding, J. Xu, Y. Yao, G. Wegner, I. Lieberwirth, C. Chen, J. Power Sourc. 192 (2009) 644–651.
[18] J. Chong, S. Xun, H. Zheng, X. Song, G. Liu, P. Ridgway, J.Q. Wang, V.S. Battaglia, J. Power Sourc. 196 (2011) 7707–7714.
[19] Y.W. Lu, X.W. Du, J. Sun, X. Han, J. Appl. Phys. 100 (2006) 063512-1–063512-4.
[20] T. Nakamura, N. Hosoya, B.P. Tiwari, S. Adachi, J. Appl. Phys. 108 (2010) 104315-1–104315-6.
[21] M.N. Obrovac, L. Christensen, Electrochem. Solid State Lett. 7 (2004) A93–A96.
[22] N. Ohta, T. Sogabe, K. Kuroda, Carbon 39 (2001) 1421–1446.
[23] R. Ruffo, S.S. Hong, C.K. Chan, R.A. Huggins, Y. Cui, J. Phys. Chem. C 113 (2009) 11390–11398.
[24] A. Guerfi, P. Charest, M. Dontigny, J. Trottier, M. Lagace, P. Hovington, A. Vijh, K. Zaghib, J. Power Sourc. 196 (2011) 5667–5673.
[25] W.C. Oliver, G.M. Pharr, J. Mater. Res. 19 (2004) 1–20.